Science and Technology Indonesia
e-ISSN:2580-4391 *p*-ISSN:2580-4405
Vol. 9, No. 2, April 2024

Research Paper

An Updated Water Masses Stratification of Indonesian Maritime Continent (IMC) Attributed to Normal and ENSO Conditions by Argo Float

Amirotul Bahiyah[1], Anindya Wirasatriya[2], Wijaya Mardiansyah[3], Iskhaq Iskandar[1,3]*

[1]*Graduate School of Sciences, Faculty of Mathematics and Natural Sciences, Sriwijaya University, Indralaya, 30662, Indonesia*
[2]*Oceanography Department, Faculty of Fisheries and Marine Science, Diponegoro University, Semarang, 50275, Indonesia*
[3]*Department of Physics, Faculty Mathematic and Natural Science, Sriwijaya University, Indralaya, 30662, Indonesia*
***Corresponding author**: iskhaq@mipa.unsri.ac.id

Abstract
The tropical area of the Indonesian Maritime Continent (IMC) is frequently regulated by El Niño-Southern Oscillation (ENSO), resulting in various water mass stratification in every climate event, such as El Niño and La Niña occurrences. As a consequence, changes in the typical Indonesian Throughflow (ITF) are linked to ENSO circumstances that affect the Indian Ocean. This study used Argo float data to evaluate the change in water mass stratification and vertical density profiles along the main pathway of ITF at each event. However, due to a scarcity of observation data, the comparison study of normal to ENSO occurrences has been limited in the ITF area. In typical circumstances throughout the year, the entrance channel (the western Pacific Ocean, the northern waters of Molucca Island, and the Halmahera Sea) had a higher saline value and cooler water masses than other ITF channels, with a range of roughly 33.5 - 35.5 PSU/13 - 22 °C, particularly during the Northwest (NW) Monsoon (December to February or DJF). Unlike the inlet, the Temperature-Salinity (T-S) diagram showed a declining value in both parameters (Celebes Sea, Makassar Strait, and Molucca Sea). Still, the outflow pathway in the Southeastern Tropical Indian Ocean (SETIO) showed a rising T-S diagram. During La Niña events, IMC water masses are often portrayed as fresher and warmer, while reverse circumstances are depicted in El Niño events with exclusion at SETIO station, indicating saltier and colder water masses than normal conditions. An extreme alteration with a large T-S range is mostly depicted in Makassar Strait from Southeast (SE) monsoon (September to November or SON) to NW monsoon, followed by the Banda Sea and then the Molucca Sea.

Keywords
ITF, Sea Stratification, Argo Float, Density Profiles, ENSO

Received: 26 June 2023, Accepted: 23 February 2024
https://doi.org/10.26554/sti.2024.9.2.299-313

1. INTRODUCTION

As the only tropical route of the global thermohaline circulation, Indonesian Throughflow (ITF) regulated the fluctuation of heat, volume, and freshwater budget in both the Indian and Pacific Ocean (Gordon, 1986; Iskandar and Suga, 2022; Lee et al., 2019; Makarim et al., 2019; Sprintall et al., 2014). As a tropical archipelago with the role of a mixed master area, the bathymetry and ocean-atmosphere process in the Indonesian Sea can modulate the incoming water mass from the Pacific Ocean. Earlier studies have shown that the incoming water masses have been modified to form a unique tropical stratification, with a comparatively isohaline structure in the thermocline layer and a very modest reduction in salinity with depth (Gordon, 2005; Iskandar and Suga, 2022; Sprintall and Révelard, 2014). The resulted modified water mass from the IMC region could affect the characteristic of Indian Ocean water mass which shows fresher and warmer water mass, particularly from the upper layer of the Indonesian sea (Iskandar and Suga, 2022).

The changing Indo-Pacific climate events, notably ENSO, can increase or reduce the ITF's involvement in ocean-atmos-phere circulation, particularly its volume transfer via heat and freshwater balance in the Indo-Pacific area on diverse time frames (Santoso et al., 2022). The tropical Pacific Ocean's climatic forcing influences the characteristics of the IMC's sea (surface-subsurface interface), causing changes to the vertical stratification of ITF flows. It is determined by Pacific waters as the water mass intake to the IMC and the quantity of radiative energy transported into the IMC's mixed layer during climate events (Kusuma et al., 2017), which is also aided by the mixing process in the IMC. The variation of ITF stratification can offer varied feedback on global climate change and Indonesian weather via the air-sea exchange (Lee et al., 2002; McCreary

et al., 2007; Potemra and Schneider, 2007; Vranes et al., 2002). Additionally, it has a considerable influence on ocean circulation and biogeochemistry (ecology) (Siswanto et al., 2021; Sprintall and Révelard, 2014). In this work, we opted to focus on the surface layer over the mixed layer, which is the most dynamic depth of the sea, since it receives a lot of direct influence from atmospheric conditions (such as radiation, wind, precipitation-evaporation), and sea surface advection during ENSO events (Iskandar and Suga, 2022; Wang et al., 2023; Mardiansyah et al., 2018; Suhadi et al., 2023; Tozuka et al., 2009; Tozuka et al., 2007).

The earliest study conducted by Wyrtki (1961) utilized the hydrographic data to evaluate the water mass characteristics within the Indonesia sea and the surrounding seas. Since then, multiple data archives, satellites, and models have been used to analyze long-term variations of the dynamics of the Indonesian Sea, revealing that the variability of the ITF water mass is exacerbated by the global hydrologic cycle (Hu et al., 2019; Iskandar and Suga, 2022; Lee and McPhaden, 2008; Li et al., 2020; Wang et al., 2023). Recent in-situ research obtained by Iskandar and Suga (2022), Guo et al. (2023), and Atmadipoera et al. (2009) utilize in-situ-based and argo-based analyses in the Indian Ocean (outlet of ITF) to calculate the outflow contribution of ITF. Argo climatology gridded data show a basin-scale freshening of Indonesian upper water (IUW) in the Indian Ocean from 2004 to 2013 and increasing trends from 2014 to 2020 which is caused by the strengthening trend of 1.33 Sv decade -1 during 1993–2018 primarily arises from salinity and secondarily from temperature of ITF. Sprintall et al. (2019) found that Indonesian stratification could be achieved by combining data from WOA 2001 and CTD. They stated that temperature, salinity, and velocity depth profiles are influenced by significant vertical mixing that varies during Indo-Pacific climatic events. However, they did not conduct any variation analysis in stratification during climate occurrences. Meanwhile, another IMC research has opted to use in-situ-based analysis for a limited area of the Indonesian-specific sea because of its capacity to disclose more particular phenomena given the paucity of in-situ data obtained by Ismail et al. (2020). His research utilized Argo float data to reveal circulation dynamics, particularly the presence of cyclonic circulation, upwelling and downwelling in the Banda Sea, and its seasonal variability of mixed layer salinity-temperature. Lu et al. (2023) utilized in-situ data from monitoring the ITF program and the Global Ocean Physics Reanalysis product to evaluate seasonal conditions from Karimata Strait to Makassar Strait and estimated the effects of salinity on the freshwater plug in Makassar Strait. The study found that halosteric factors account for roughly (69.6 ± 11.7) % of the total seasonal variability in surface dynamic height gradient in the Makassar Strait, mostly affecting the top layer.

Either the integration of satellite-model data in the IMC is used to highlight a longer pattern of IMC circulation or to relate it to Indo-Climate events using time series data. Previous studies by Hu and Sprintall (2016) and Santoso et al. (2022) linked ITF variability to ENSO and IOD via anomalous Indo-Pacific Walker circulation, utilizing a mix of in-situ observations, reanalysis, and model data. They emphasize the relevance of the ITF's vertical structure, which responds differently to ENSO and the IOD; hence, diagnosing the ITF's changes under different climatic conditions involves taking into consideration activities in the various layers (Santoso et al., 2022). In addition, the ENSO has a stronger influence on total ITF transit than the Indian Ocean Dipole (Hu and Sprintall, 2016). Zhu et al. (2019) employed the Hybrid Coordinate Ocean Model+Navy Coupled Ocean Data Assimilation Global Analysis (GLBa0.08) in the Banda Sea to emphasize vorticity distribution within a four-layer structure, which is greater in the upper 700 m than in deeper layers. They discovered that monsoonal winds mostly drive the middle and eastern Banda Sea circulation, but Coriolis force dominates the western and southern limits. Furthermore, Halkides et al. (2011) used model data from the ECCO ocean-state estimate along with satellite data to calculate the mixed layer thermal budget (seasonally dominated by surface heat flux) and mixed layer salinity (seasonally dominated by advection) in the Banda Sea.

However, studies on the vertical profiles of the ITF water mass under the impact of ENSO event using in-situ data have not been detailly updated, particularly along the ITF path from the entrance area, within the Indonesian seas, to the exit area in the SETIO region. In order to fill this gap for a better understanding on the variability and dynamics of vertical profiles of the ITF water mass, we analyzed 8 Argo data using T-S diagram analysis along the ITF pathway. The rest of this paper is organized as follow. Section 2 explains the dataset and methodology used in this study. Section 4 presents main finding of this study, and Section 5 concludes our results.

2. EXPERIMENTAL SECTION

2.1 Study Area

The area of interest is along the ITF pathway, including the western equatorial Pacific Ocean, the northern waters of Moluc -ca Island, Celebes/Sulawesi Sea, Halmahera Sea, Moluca Sea, Makassar Strait, Banda Sea, and the SETIO region (Figure 1). As reported in the previous study, the main route of incoming ITF water is the Makassar Strait (Gordon and Fine, 1996; Iskandar and Suga, 2022; Sprintall and Révelard, 2014). The second incoming ITF pathway is through the northern channel of the Banda Sea including the Halmahera Sea and Lifamatola Passage (Gordon and Fine, 1996; Sprintall et al., 2014; van Aken et al., 2009). The last pathway is in the western Indonesian sea through the Karimata Strait (Lee et al., 2019; Sprintall et al., 2014). Note that the incoming ITF water mass is gathered in Banda Sea (Gordon and Susanto, 2001; Napitu et al., 2015). Meanwhile, the outflow ITF pathways are through the Lombok Strait, Ombai Strait, and Timor Passage (Iskandar and Suga, 2022; Sprintall et al., 2014; Sprintall et al., 2009).

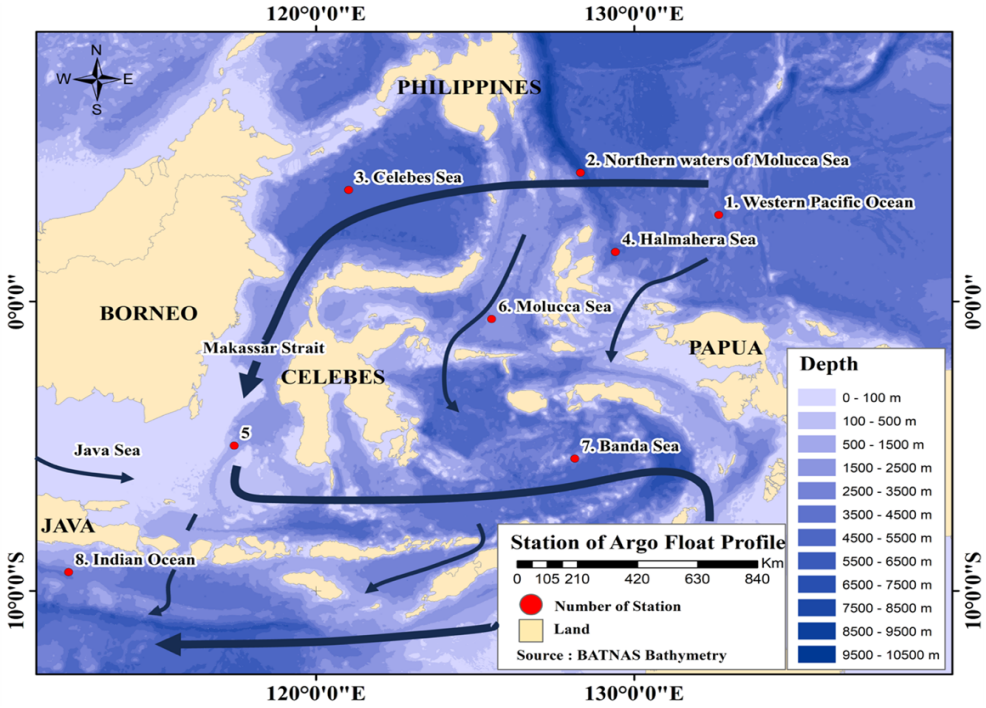

Figure 1. The Research Area along the ITF Pathway, Including the Western Pacific Ocean, the Indonesian Seas and the Southeastern Tropical Indian Ocean. The Red Points Are the Starting Location of the Argo Float Trajectory. The Bathymetry of the Ocean Is Shown by the Blue-Color Degradation Which Is Obtained From the Bathymetry Reclass BATNAS

2.2 Data

2.2.1 Argo Float Data

In order to illustrate the spatial variability of the vertical profile of the ITF water mass, we utilized the Argo float data within the period of 2013 to 2022 (Table 1). The Argo float data is a part of the global series free-float buoys which measured subsurface temperature, salinity, and pressure vertically in the upper sea layer above 2000 m depth. A comprehensive data set that were collected approximately 150,000 profiles annually provided a continuous data record of the world's oceans since 2000 (Holte et al., 2017). In addition, the individual data have the capability in describing the mixed layer depth (MLD) the distribution of barrier layer thickness (BLT), and its energetic globally in 10-day intervals at specific regions of interest (Agarwal et al., 2012; Hosoda et al., 2010). Moreover, the Argo profile is also long enough to illustrate MLD intra-seasonal variations (Drushka et al., 2012; Keerthi et al., 2013). The vertical resolution of these floats is roughly 10 m in the upper layer of 200 m (Agarwal et al., 2012). The data can be downloaded through the https://www.nodc.noaa.gov/argo/floats_data.htm.

2.3 Methods

2.3.1 Climate Mode in the Tropical Pacific Ocean

In this study, we evaluated the possible impact of the climate mode originated from the tropical Pacific Ocean, namely the El Niño and La Niña events to the ITF water mass. We defined the normal, El Niño, and La Niña events using the Niño 3.4 index for the period of 2008 to 2022. Then, the Argo data are classified based on these events. Note that this time division of the Argo data follows the period of El Niño/ La Niña evolution from May to June of the following years. In addition, we also divided the Argo data based on the season, that is September–October–November (SON) for the beginning phase of evolution, and December–January–February (DJF) for the peak phase of the evolution. Meanwhile, the diminishing phase of evolution is not observed as it is believed to have reserved conditions of the beginning of evolution in each event.

2.3.2 Niño Index

Niño 3.4 index is a partial area of the tropical Pacific Ocean representing the oceanic evolution of the El Niño or La Niña events that has a relation to climate variability in the Maritime Continent. Its region stretched from 5° N to 5° S and 120° to 170° W (Iskandar et al., 2019; Iskandar et al., 2018; Jin and Wright, 2020; Setiawan et al., 2020). We calculated the Niño 3.4 index based on the Optimum Interpolation Sea Surface Temperature (OISST) data (Figure 2). The OISST data have a spatial resolution of about 0.083° × 0.083° km. The data is produced and maintained by the National Climate Data Center (NCDC) of the National Oceanographic and Atmospheric Administration (NOAA) (Banzon et al., 2016). Monthly climatology of the SST data is calculated for the period of January 2002 to December 2021, and then the monthly SST anomaly

Table 1. Data of Argo Used in the Present Study with a Period of 2013 to 2022

Station	Argo Float Profile
1st station	nodc_5904699_prof, nodc_5904526_prof, nodc_2901548_prof, nodc_5904051_prof
2nd station	nodc_5904526_prof, nodc_2902845_prof, nodc_2902738_prof, nodc_5904907_prof, nodc_5904020_prof, nodc_5904309_prof
3rd station	nodc_5902335_prof, nodc_2902729_prof, nodc_5902335_prof, nodc_2901518_prof, nodc_5904306_prof, nodc_5903748_prof
4th station	nodc_5904865_prof, nodc_5904367_prof, nodc_5904377_prof, nodc_5904051_prof
5th station	nodc_5904965_prof, nodc_5903451_prof, nodc_5901590_prof
6th station	nodc_5904508_prof, nodc_5904531_prof, nodc_5904961_prof
7th station	nodc_6901746_prof, nodc_6901747_prof
8th station	nodc_5905017_prof, nodc_5905020_prof, nodc_5905021_prof, nodc_5902608_prof, nodc_5903915_prof, nodc_5903949_prof

is defined as the deviation from its monthly climatology (Iskandar et al., 2017). The El Niño events are defined when the index is greater than 0.5 °C for at least five consecutive months, while the La Niña events are determined when the index is less than −0.5 °C for at least five consecutive months (Jin and Wright, 2020).

2.3.3 The Thermal Layers

In order to illustrate the subsurface layer dynamics of the ITF water, we analyze the MLD, Isothermal Layer Depth (ILD), and Barrier Layer Thickness (BLT) based on the T-S diagram generated for each ARGO data. Previous studies have defined the MLD as the depth (D) where the potential density changes relative to the reference density at a depth of 5 m by defining the depth of salinity changes of about 0.2 PSU (de Boyer Montégut et al., 2007; Drushka et al., 2010; Kara et al., 2000; Sprintall and Tomczak, 1992). Meanwhile, the ILD is determined using a depth (D) where the temperature experiences a decrease reaching the threshold ΔT = 1.0 °C below the reference temperature or sea surface temperature at a depth of 5 m or $T_{(ref)} = T_{(D=5)}$. Those two parameters are calculated by using the following equations,

$$ILD = D|_{T_{ref} - \Delta T} \quad (1)$$

$$MLD = D|_{\sigma\theta = \sigma\theta(D=5) + \sigma\theta} \quad (2)$$

The change in potential density used in terms of the density (P) value at the depth of the ILD, which is impacted by the reduction in temperature (T), to the density at the reference depth, provided the salinity remains constant:

$$\Delta\sigma_\theta = \sigma_\theta(T_{ref} - \Delta T, S_{ref}P_0) - \sigma_\theta(T_{ref}, S_{ref}, P_0) \quad (3)$$

where S_{ref} is salinity (S) at a reference depth of 5 m and P_0 is the pressure at sea level. BLT is defined as the thickness of the barrier layer which indicates the difference between ILD and MLD depths (Agarwal et al., 2012; Sprintall and Tomczak, 1992) and it is defined as,

$$BLT = ILD - MDL \quad (4)$$

3. RESULTS AND DISCUSSION

3.1 ENSO Events during 2002-2022

ENSO is a coupled ocean-atmosphere phenomenon originated from the tropical Pacific Ocean that has two phases, namely the cold phase (El Niño) and the warm phase (La Niña). Previous studies have shown the impact of ENSO events on the Maritime Continent in which the El Niño (La Niña) event causes deficit (excess) rainfall over the Maritime Continent (Aldrian and Dwi Susanto, 2003; Yulihastin and Febrianti, 2009; Supari et al., 2018; Iskandar et al., 2019). The influence of ENSO on the Maritime Continent extends beyond direct meteorological effects. Changes in SST and rainfall patterns associated with the ENSO event can affect the distribution and abundance of fish species, potentially leading to shifts in fishing ground and impacting the income of local fishermen (Syamsuddin et al., 2013). Therefore, the ENSO events exert a profound influence on the Maritime Continent, shaping weather patterns, impacting marine ecosystems, and influencing the livelihoods of coastal communities.

As shown in Figure 2, there was a very strong El Niño event in 2015/2016, with Niño 3.4 index reaching more than 2.5 °C. There were also two moderate El Niño events observed in 2009/2010 and 2019/2020. On the other hand, there were four La Niña events observed during the period of analysis, which were 2007/2008, 2010/2011, 2011/2012 and 2020/2021.

3.2 Water Mass Stratification of the ITF in Normal Conditions

Indonesian Sea is the only tropical sea having a role in linking water masses between the Pacific Ocean and the Indian Ocean (Lee et al., 2019) which is forced by the pressure gradient between those two oceans (Wyrtki, 1987). This pressure gradient is associated with the trade winds over the tropical Pacific Ocean and the monsoon winds over the Maritime Continent

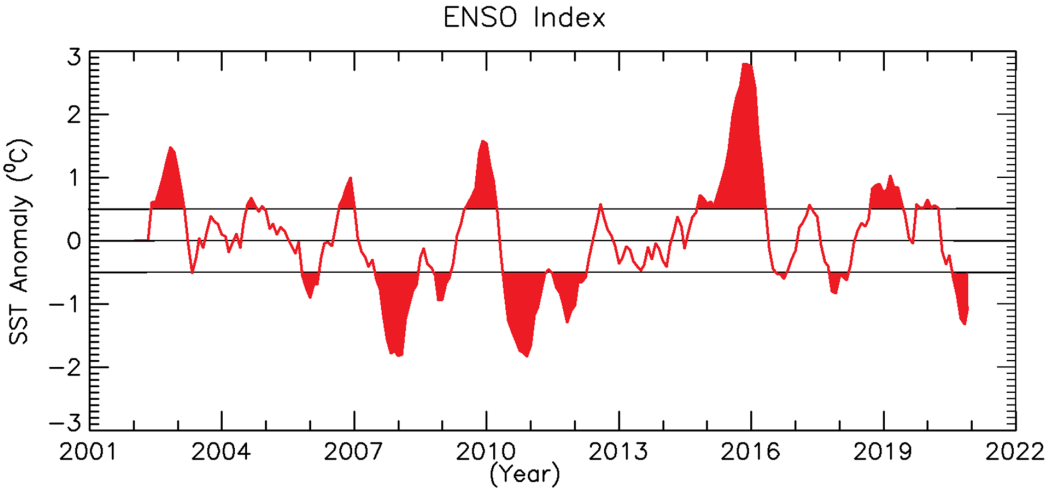

Figure 2. Time series of the Niño 3.4 Surface Temperature Anomaly (SSTA) between 50° N and 50° S, and 120° W to 170° W. El Niño (La Niña) Occurs when the Index Exceeds or Falls below 0.5 °C (-0.5 °C) for Five Months in a Row, as Indicated by the Red Shading

(Li et al., 2020; Potemra and Schneider, 2007). Moreover, the ITF is a part of the global thermohaline circulation, where it plays an important role in the upper layers of the global reverse circulation (Feng et al., 2018; Gordon, 1986). The ITF transports warm and fresh water from the Pacific to enter the Indian Ocean through the Indonesian seas, particularly in the upper layer of the ocean around 300 m depth. As a result, the ITF could regulate the Indian Ocean stratification and surface heat flux (Song and Gordon, 2004).

Figure 3 shows the vertical profile of the ITF along its pathway based on the T-S diagram during a normal year without any influence from El Niño nor La Niña event. Previous studies have suggested that the vertical stratification of water masses from the Pacific Ocean entering the Indonesia seas is altered by strong air-sea fluxes, monsoonal wind-induced upwelling, bottom sea topography, and extremely large tidal force during the travel in the Indonesian sea (Koch Larrouy et al., 2008; Sprintall and Révelard, 2014). The annual mean of water mass stratification reveals that water mass becomes fresher as it travels from the Pacific Ocean to the Indian Ocean via the ITF pathway (Figures 3a and 3b). Interestingly, the ITF profiles reveal a distinct pattern in each monsoon season (Figures 3c-d). In particular, robust upper layer freshening was observed within the Indonesian seas south of the Makassar strait during the northwest monsoon season (Figure 3d). This result confirms previous findings which suggested that the upper layer freshening in the southern part of the Makassar Strait is resulted in from the incoming freshwater from the Java Sea associated with high precipitation over the Maritime Continent during the northwest monsoon season (Lee et al., 2019; Bahiyah et al., 2019). In addition, small alteration in the vertical profiles of the ITF along its pathways was also observed in the deeper layer during different seasons (Figures 3c-d).

In order to illustrate the vertical freshening and warming/cooling by ocean processes along the ITF pathway, we then analyzed the Argo float time-series data in the upper 300 m (Table 2). As can be seen that the T-S diagram as well as its values of inlet stations (stations 1, 2, and 4 –see also Figure 1) is found in a different pattern and values than those of the Indonesian sea stations (station 3, 5, 6 and 7) and outlet station (station 8). The Pacific Ocean (station 1), the first inlet of the ITF in the north of Molucca Sea (station 2), and the Halmahera Sea (station 4) have a higher salinity value in the upper layer of around 33.5 – 35.5 PSU with a different salinity value from Pacific Ocean to the inlet of ITF are about 0.1 - 0.5 PSU. The temperature values are about 20 – 31 °C in the upper layer, while they are about 11 – 22 °C around 200 m depths. Relatively fresher and warmer water masses were observed in the south of Makassar Strait (station 5). However, station 6 reveals slight freshening in the upper 100 m depth of around 33.7 – 34.6 PSU, while the temperature is about 19 – 30 °C. Meanwhile, in the deeper layer around 200 m, the salinity and temperature values observed at both of stations (stations 5 and 6) reveal almost no change as its incoming water in the inlet stations. As the outlet, Indian Ocean is affected by ITF water masses. During normal conditions, the Indian Ocean shows a low salinity value of around 32.8 – 35.3 PSU with colder temperatures of 16 – 30 °C in the upper layer of 100 m, and 10 – 24 °C in the deeper layer of 200 m depth. This result is in agreement with the previous study which suggested the cooling process of the ITF water within the Indonesian sea before it flows into the Indian Ocean (Gordon, 2005).

During SON to DJF seasons, salinity level in stations 1, 2, 3, and 4 increases by around 0.1 to 1.0 PSU from SON season to DJF season, while the temperature decreases with a minimum value of around 18 °C in the western Pacific Ocean and 22 °C in the Halmahera Sea. Interestingly, within the Indonesian seas (stations 5 and 6) we found a decreasing salinity

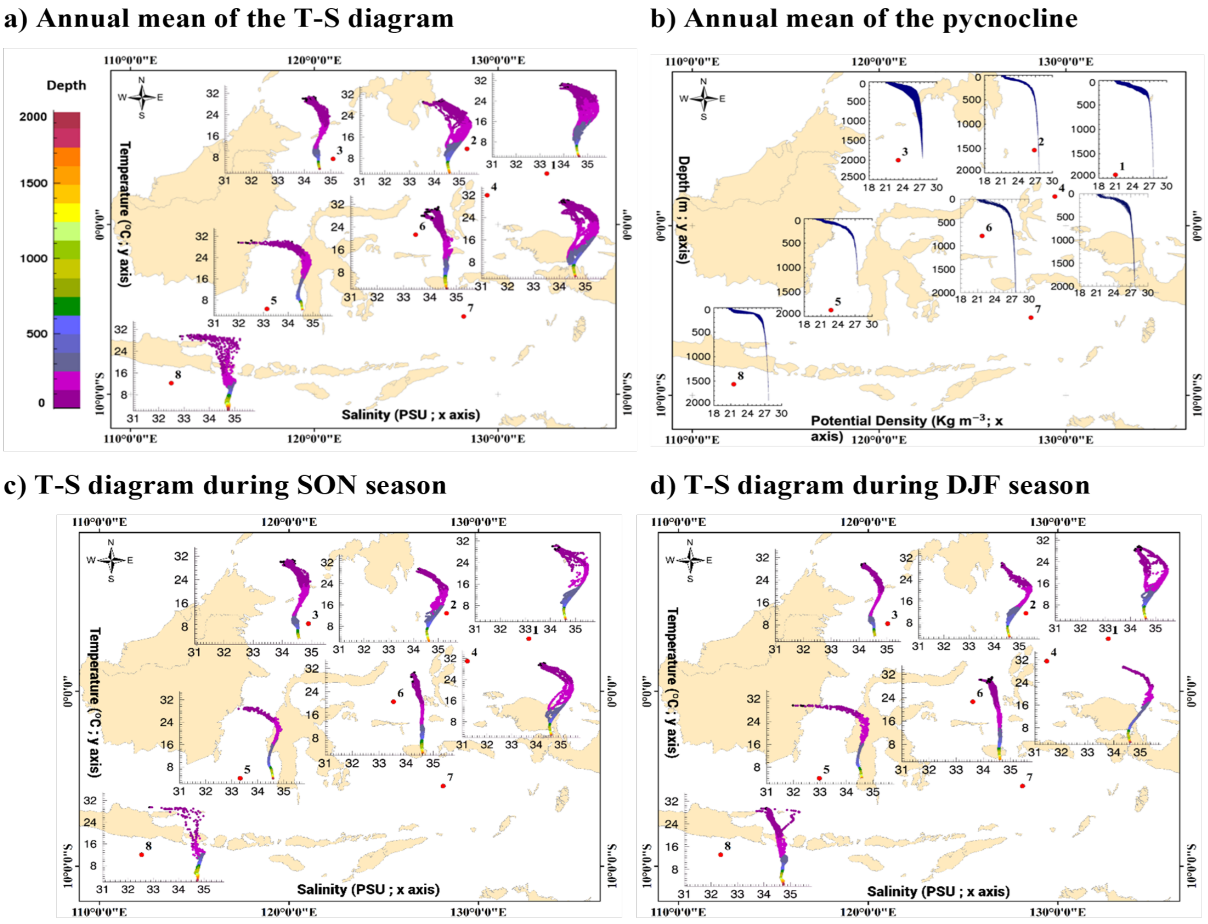

Figure 3. Annual Mean of a) T-S Diagram, and b) Pycnocline Profile Derived from the Argo Floats within the Indonesian Seas during the Normal Conditions. Seasonal Averaged of the T-S Diagram during c) Southeast Monsoon (SON), and d) Northwest Monsoon (DJF). Each of T-S Diagram Shows Salinity in PSU Unit on the x-Axis, Temperature in °C Unit on the y-Axis and Colour Gradation Represents Depth Magnitude in Meters for z-Axis. The Upper Layer in the Depth of 200 m Is Depicted by Purple Color and the Deeper Layer is Shown as Blueish to Reddish. Meanwhile, the Pycnocline Profile Shows Potential Density with the Units of kg.m^{-3} in x-Axis and Depth (m) in the y-Axis

and temperature from SON season to DJF season with the minimum value of around 33.8 PSU to 32 PSU at station 5, and 34.1 PSU to 33.9 PSU at station 6. The Indian Ocean stratification (station 8) shows increased values both of salinity and temperature during the transition of SON to DJF. The minimum value of salinity is around 33 PSU (SON) to 33.7 PSU (DJF), while the minimum temperature of 16 °C during SON becomes 18 °C during DJF. However, the Indian Ocean represented by station 8 is less saline during the northwest monsoon as shown by the shape and pattern of T-S diagram (Figures 3c-d).

Time-depth density plots overlaid with MLD and ILD capture several ocean processes (Figure 4). The density profile of the Pacific Ocean depicted few fluctuations during from SON season to DJF season and reveals shallow MLD and ILD. The time-depth density profile in the Pacific Ocean (inlet station) reveals very low variability in both ILD and MLD and relatively steadies upper layer structure of the vertical density. On the other hand, robust seasonal variation of both ILD and MLD was observed in the Makassar Strait and the Indian Ocean sites. The northwest monsoon has a deeper thermocline layer, while the southeast monsoon has a shallower thermocline layer. The typical pattern of ILD during the southeast monsoon is shallower about 40 m than that during the northwest monsoon which reaches about 80 m. In the Makassar Strait, very low density in the upper layer was observed during the northwest monsoon reaching about 1020.0 kg/m^3. This condition depicts the appearance of freshwater input in this area (middle panel of Figure 4). This freshening is also depicted by shallow MLD and deeper ILD resulted in a thick barrier layer during the northwest monsoon compared to other monsoon seasons. However, the upwelling process was also depicted during the

Table 2. Water Mass Stratification along the ITF Pathway during Normal Conditions. This Table Is Based on the T-S Diagrams in Figure 3 Showing Annual Mean of the T-S Diagrams in the Depth of 100 m and 200 m. It Also Provides Seasonal Patterns during SON and DJF in the Depth of 100 m

Stations	Annual Mean in the Upper Depth of 100 m		Annual Mean in the Depth of Around 200 m		T-S Range of Upper 100 m Depth during DJF		T-S Range of Upper 100 m Depth during SON	
	Salinity (PSU)	T (°C)	Salinity (PSU)	T (°C)	Salinity (PSU)	T (°C)	Salinity (PSU)	T (°C)
Station 1	33.9 - 35.4	20 - 31	34.4 – 35.7	10 - 22	34.0 – 35.4	18 - 30	33.9 – 35.4	21 - 30
Station 2	33.5 -35.5	20 - 31	34.4 – 35.5	13 - 22	34.2 – 35.5	21 - 30	34.1 – 35.3	22 - 30
Station 3	33.9 – 34.9	21 - 31	34.3 – 35.0	11 - 22	34.0 – 34.9	18 - 30	34.0 – 35.0	19 - 30
Station 4	34.0 – 35.5	20 - 31	34.3 – 35.4	13 - 22	34.3 – 35.4	22 - 30	33.9 – 35.5	22 - 30
Station 5	32.0 – 34.7	25 - 30	34.4 – 35.0	16 - 25	32.0 – 34.4	25 - 30	33.8 – 34.7	26 - 30
Station 6	33.7 – 34.6	19 - 30	34.5 – 34.8	13 - 19	33.9 – 34.6	19 - 30	34.1 – 34.6	20 - 30
Station 7	Nan	Nan	Nan	Nan	Nan	Nan	Nan	Nan
Station 8	32.8 – 35.3	16 - 30	34.5 – 35.1	10 - 24	33.7 – 35.3	18 - 30	33.0 -35.2	16 - 30

Table 3. Water Mass Stratification of IMC in All Stations during La Niña Events. This Table Is Similar to Table 2, however, It Is Based on the TS Diagram in Figure 5

Stations	Annual Mean in the Upper Depth of 100 m		Annual Mean in the Depth of Around 200 m		T-S Range of Upper 100 m Depth during DJF		T-S Range of Upper 100 m Depth during SON	
	Salinity (PSU)	T (°C)	Salinity (PSU)	T (°C)	Salinity (PSU)	T (°C)	Salinity (PSU)	T (°C)
Station 1	33.4 – 35.5	20 - 31	34.4 – 35.6	10 - 26	34.2 – 35.4	25 - 30	33.8 – 35.0	25 - 30
Station 2	33.3 – 34.8	21 - 30	34.5 – 35.3	12 - 27	33.3 – 35.0	20 – 30	33.6 – 35.0	21 - 30
Station 3	33.1 – 35.0	21 - 31	34.4 – 34.9	12 - 25	33.2 34.8	20 - 30	33.8 – 34.8	19 - 30
Station 4	33.7 – 35.5	25 - 31	34.6 – 35. 7	14 - 27	33.9 – 35.0	28 - 31	33.9 – 35.2	25 - 31
Station 5	31.0 – 34.0	28 - 31	32.9 – 34.7	18 – 30	31.0 – 33.8	26 - 30	33.0 – 34.0	27 - 31
Station 6	32.5 – 35.6	22 - 31	34.2 - 35.9	11 - 27	32.5 – 35.2	21 - 30	33.8 – 35.6	23 - 31
Station 7	33.2 – 34.4	23 - 31	34.1 – 34.6	18 - 28	33.7 – 34.1	27 – 31	33.8 – 34.4	24 - 30
Station 8	32.6 – 35.2	17 - 30	34.5 - 35	11 - 17	33.6 – 35.1	15 - 29	33.0 – 34.8	17 - 28

monsoon break (March-April-May/MAM) where the ILD in this area reached of around 10-20 m. On the other hand, the downwelling process was captured in Indian Ocean during the northwest monsoon, particularly from January to February (lower panel of Figure 4) as well as high temperature and low salinity in T-S diagram (Figure 3d). This area is believed as the convergence area of different water masses from the Indian Ocean and the ITF, indicated by deep MLD and ILD of around 100-120 m. A recent study showed that higher salinity is coming from the tropical Indian Ocean, which is driven by wind and associated with the south Java current of around ~1 Sv, while the higher temperature is influenced by the ITF water masses input (Guo et al., 2023). Note that during the northwest monsoon, the ITF water masses are influenced by river runoff and the South China Sea that are characterized by lower salinity and warmer water masses, particularly in their southern hemisphere (Meehl, 1987; Napitu et al., 2015; Tanaka, 1994).

3.3 The Water Mass Stratification during the La Niña Event

Upper layer (a mixed layer) is the most dynamic layer due to being coupled with atmospheric flux. It has been suggested that the ITF transport mostly occurs in the thermocline around 200 m (Gordon et al., 2010; Wang et al., 2023). During La Niña events, the ITF water masses are categorized in fresher water than during normal conditions. The increasing temperature occurs during this event, as the impact of warm water pool propagates to the west of Pacific Ocean nearby the IMC. These typical conditions are illustrated by the curve of TS-diagram, namely the upper layer in Pacific Ocean is dominated by warmer waters with a temperature of about 27 °C and lower salinity of around 33.4 – 35.5 PSU. As the effect of the Pacific Ocean alterations, the domination of IMC waters stratification also showed to be warmer and lower salinity levels in the upper layer. The decreasing ocean parameters in most ITF pathways reach 1-5 °C (temperature) and 0.2 – 2 PSU (salinity) as illustrated in Figure 5a. Focusing on the upper layer, stations 1 to 2 and 3 have a few different ranges of temperature around 1 °C, and salinity of around 0.1 – 0.7 PSU. The main pathway of ITF (station 5) has warmer and fresher waters around 28 – 31 °C than other Indonesian seas.

Here we provided Figure 5 to illustrate a typical stratification of IMC during La Niña anomalies from in-situ data. Similar to the previous picture, we provided a TS-diagram (Figure 5a) with its pycnocline attribute (Figure 5b) along the year to illustrate the typical ocean attributes along ITF pathways and their modification based on distinct monsoon seasons (Figures 5c and 5d).

Table 4. Water Mass Stratification of IMC in All Stations during El Niño Events. This Table Is Similar to Tables 2 and 3, which is based on the TS Diagram in Figure 5

Stations	Annual Mean in the Upper Depth of 100 m		Annual Mean in the Depth of Around 200 m		T-S Range of Upper 100 m Depth during DJF		T-S Range of Upper 100 m Depth during SON	
	Salinity (PSU)	T (°C)	Salinity (PSU)	T (°C)	Salinity (PSU)	T (°C)	Salinity (PSU)	T (°C)
Station 1	34.0 -35.4	19 - 30	34.4 – 35.4	11 - 23	34.7 – 35.3	21 - 31	34.3 – 35.3	22 - 31
Station 2	33.9 – 35.2	16 - 30	34.3 – 35.0	9 - 22	34.3 – 35.3	15 – 30	34.1 – 35.2	17 - 31
Station 3	33.6 – 35.0	17 - 31	34.4 – 35.2	14 - 24	34.2 – 35.0	17 - 31	33.7 – 35.2	18 - 30
Station 4	33.9 – 35.3	17 - 30	34.4 – 35.4	11 - 24	34.3 – 35.3	15 - 31	34.5 – 35.3	20 - 31
Station 5	33.5 – 34.4	25 - 30	34. 0 - 34.7	20 - 29	33.6 – 34.0	30 - 31	33.7 – 34.4	27 - 31
Station 6	33.2 – 34.5	21 - 30	34.4 – 34.9	13 - 24	33.8 – 34.6	20 - 31	33.9 – 34.6	21 - 31
Station 7	32.6 – 34.5	27 - 31	33.9 – 34.5	20 - 27	34.1 – 34.4	30 - 31	34.1 – 34.4	23 - 31
Station 8	32.8 – 34.9	18 - 31	34.5 – 34.8	13 - 20	33.2 - 34.9	15 - 30	34.2 – 35.0	16 - 30

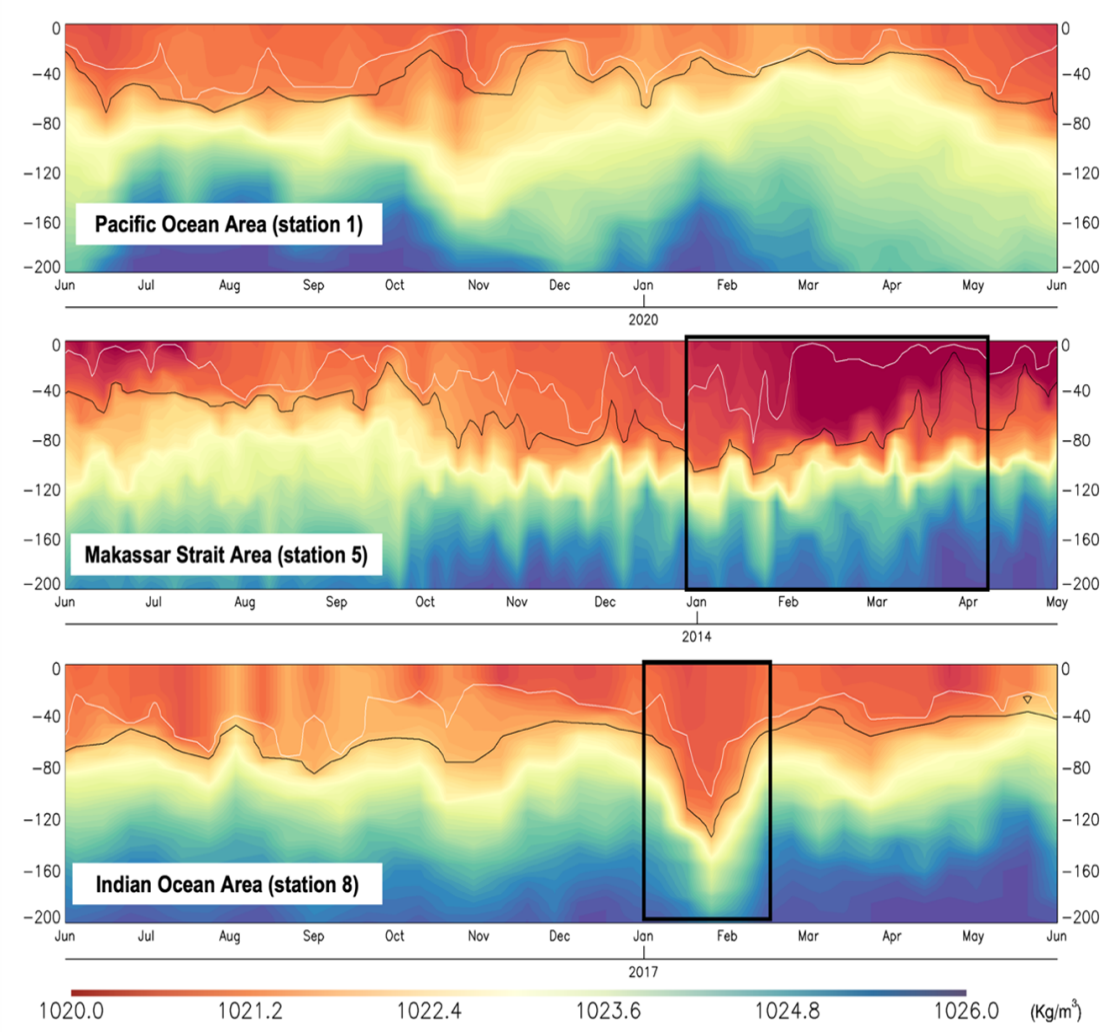

Figure 4. Time-Depth Density Profiles in the Upper 200 m along the ITF patways: a) in the Tropical Pacific, b) within the Indonesia Sea (the Makssar Strait), and c) in the Indian Ocean. The MLD and ILD Are Shown in White and Black Lines, Respectively

Increasing temperature and decreasing salinity occurred not only in the surface layer, but also in the deeper layer at 200 m, as shown at stations 1, 2, 3, 4, 5, and 8 (Table 3). Station 8 has the most dramatic salinity and temperature variation, ranging

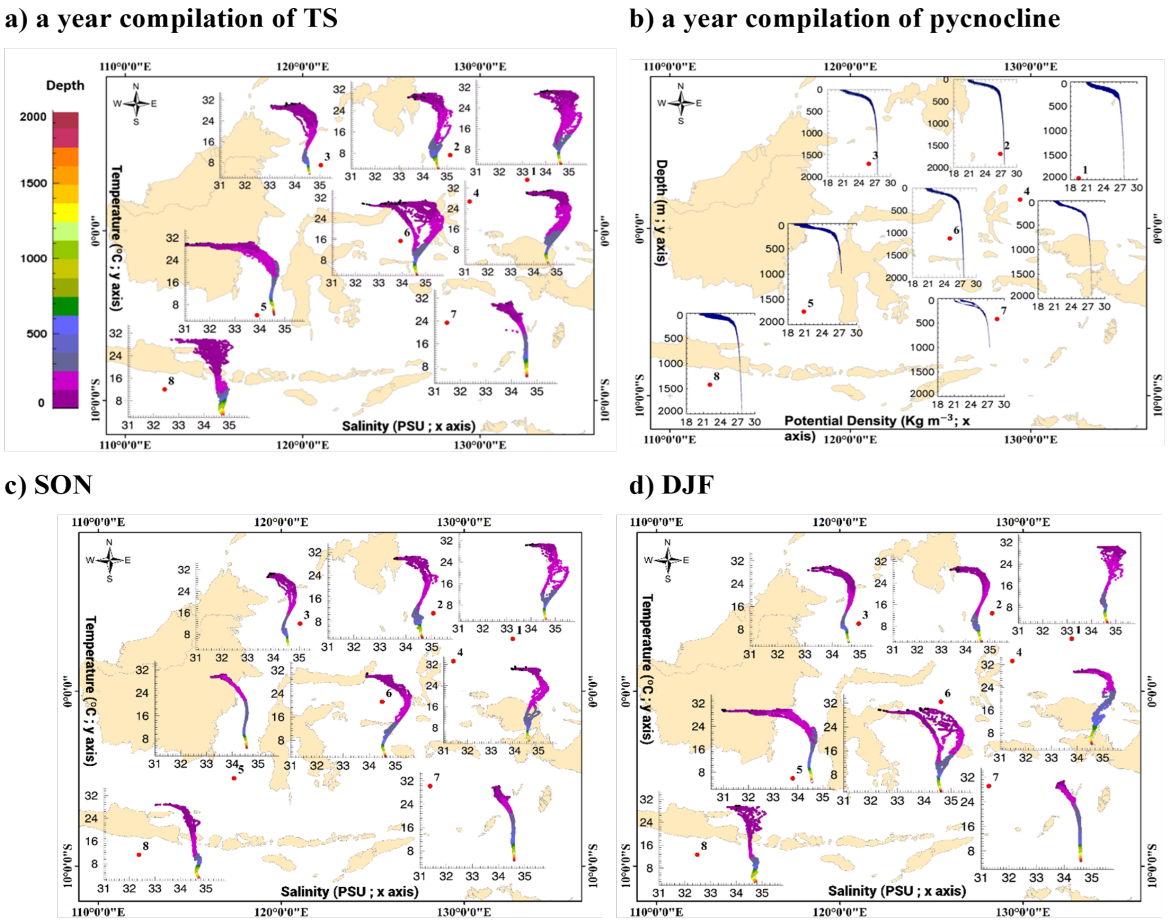

Figure 5. Annual Pattern of a) TS Diagram and b) Pycnocline Profile by Argo Float in IMC during the Period of La Niña events. Seasonally Conditions Are Depicted by Figure c) Stratification of Water Masses during SON and Figure d) Stratification of Water Masses during DJF. Each of TS Diagram Shows Salinity in PSU Unit on the x-Axis, Temperature in °C Unit on the y-Axis and Colour Gradation Represents Depth Magnitude in Meters for z-Axis, meanwhile, for Pycnocline Profile Shows Potential Density with the Units of kg.m^{-3} in x-Axis and Depth (m) in the y-Axis

from 34.5 - 35.1 PSU/ 10 - 24 °C (typical circumstances) to 32.9 - 34.7 PSU/18-30 °C. Station 6 is shown to have a warmer temperature and a higher salinity value of 34.2 - 35.9 PSU/11-27 °C compared to the typical circumstances of 34.5 - 34.8/13 - 19 °C. The anomaly is also seen at station 8, where the temperature in 200 m is around 11 - 17 °C lower than typical circumstances, with a difference of 1-5 °C. However, the salinity value in the event was close to typical circumstances, ranging from 34.5 to 35 PSU. Salinity and temperature changes between stations 1, 2, 4, and 6 are minor, ranging from 1-2 °C and 0.1 - 0.3 PSU in the deeper layer. Stations 3 and 7 exhibit salinity readings ranging from 34.1 to 34.6, whereas the difference in salinity between Makassar Strait-Java Sea and Banda Sea is around 0.3 PSU.

The TS diagram shows in detail how water shifts from SON to DJF in the IMC (Figures 5b and 5c). SON represents the early stages of ENSO (Figure 5c), whereas DJF (Figure 5d) represents the peak time of ENSO occurrences. Typical salinity characteristics in the Pacific Ocean during peak season in this event include an increase in salinity of 0.4 - 0.5 PSU from SON to DJF at the same temperature. Stations 2, 3, 4, 5, 6, and 7 indicate decreasing salinity levels ranging from 0.2 to 2.0 PSU. Meanwhile, station 8 has a greater salinity value ranging from 33.0 - 34.8 PSU (SON) to 33.6 - 35.1 PSU (DJF), as well as a broader temperature range of 2 - 3 °C during the peak time. However, the temperature in each station observed a distinct pattern, with stations 1, 2, and 3 being steady, stations 4 and 7 showing rising temperatures, and stations 5, 6, and 8 having lower temperature values. Among these stations, an extreme decrease in salinity and temperature alterations occurred in the Banda Sea and Molucca Sea stations, with values ranging from SON 33.0 - 34.0 PSU/27 - 31 °C (station 5) and 33.8 - 35.6 PSU/23 - 31 °C (Station 6) to DJF around 31.0 - 33.8 PSU/26 - 30 °C (Station 5) and 32.5 -

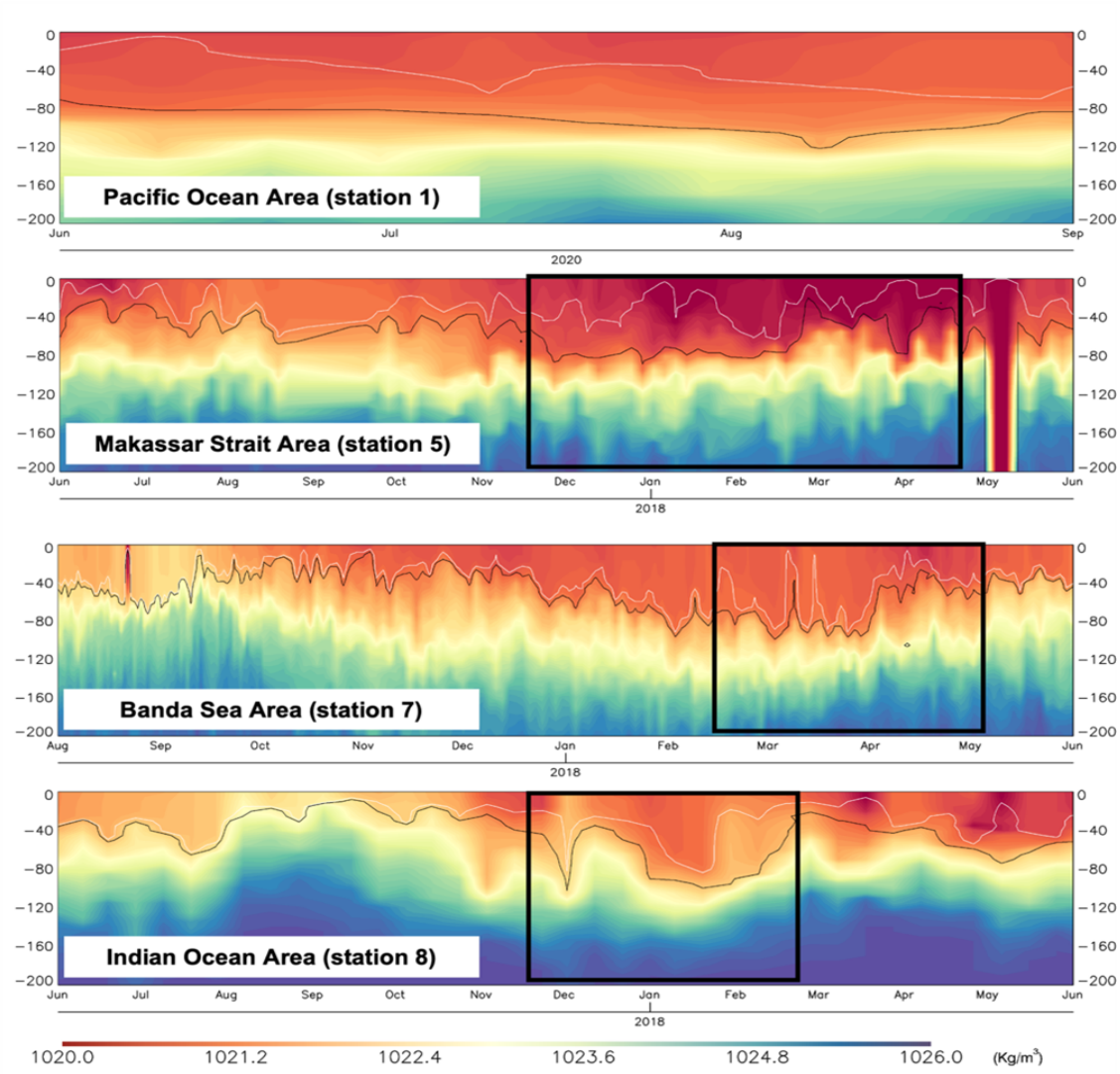

Figure 6. Density Profile in Several ITF Pathways during La Niña Events, Particularly in the Pacific Ocean as the Inlet Area, Makassar Strait as the Main Pathways of ITF, Banda Sea as the Transit Area of Most ITF Water Mass, and Indian Ocean as the Final Route. This Time-Depth Illustration Shows Vertical Profile of Density Based on TS Diagram in the Figure 5. The density Profile Is Overlaid with MLD in White Line and ILD in Black Line. Density Profile Is Measured in the Kg.m^{-3} Units where the Lower Pressure Is in the Upper Layer with Reddish Shade

35.2 PSU/21 - 30 °C (station 6).

The density profile in Figure 6 reflects a similar pattern to the TS diagram, which also depicts upper-layer dynamics. During La Niña events, the Pacific Ocean maintains a constant ILD of 80-120 m, whereas MLD fluctuates between 0-80 m in early 2020. During the northwest monsoon (peak times of ENSO events), a deeper layer of depth component (MLD and ILD) is illustrated in the Makassar Sea, Banda Sea, and Indian Ocean, with a depth of around 80 m in the Makassar Strait and 100-120 m in the Banda Sea and Indian Ocean. Moreover, other anomalies are visible in various areas of Figure 6, such as thick BLT exhibited during DJF in Makassar Strait, MAM in Banda Sea, and February in the Indian Ocean. Furthermore, an upwelling process in Makassar Strait and a low upwelling process in the Banda Sea occurred during the northwest monsoon (MAM), whereas a downwelling process appeared in the Indian Ocean during DJF. BLT is a property of freshwater in the upper seas, whereas downwelling (upwelling) is a feature of convergent (divergent) water masses. Several hypotheses were developed in this study based on the TS diagram pattern and density profile at all stations, including the Banda Sea having a pattern similar to the Arafura Sea and the Indian Ocean having a pattern similar to the Makassar Strait.

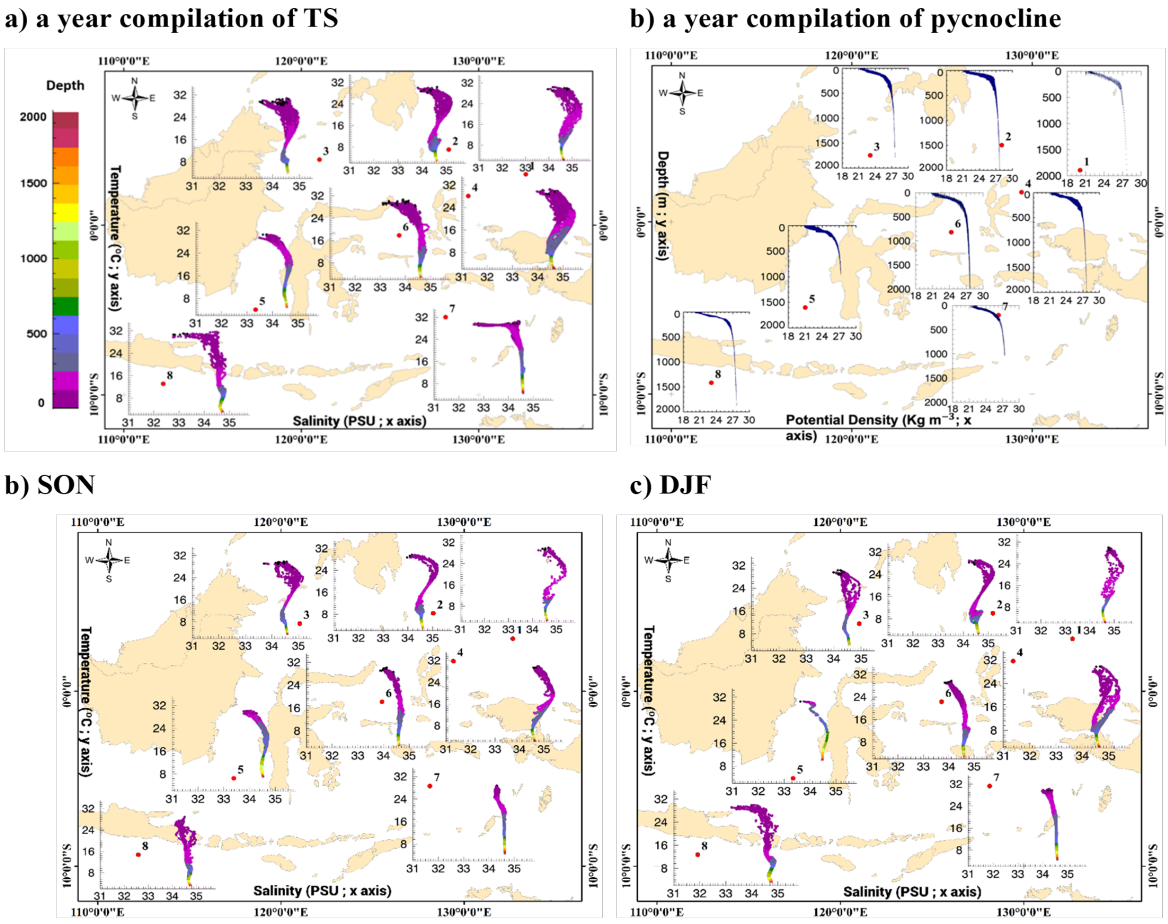

Figure 7. Annual Pattern of a) TS Diagram and b) Pycnocline Profile by Argo Float in IMC during the Period of El Niño Events. Seasonally Conditions Illustrate by Figure c) TS Diagram during SE Monsoon (SON) and Figure d) TS Diagram during NW Monsoon (DJF). Each of TS diagram shows salinity in PSU unit on the x-Axis, Temperature in °C Unit on the y-Axis and Colour Gradation Represents Depth Magnitude in Meters for z-Axis. Meanwhile, for Pycnocline Profile Shows Potential Density with the Units of kg.m^{-3} in x-Axis and Depth (m) in the y-Axis

3.4 The Water Mass Stratification during the El Niño Event

During El Niño occurrences, IMC water masses in a year compilation (Figure 7a and 7b) tend to be cooler (decreasing approximately 1 - 8 °C) with the pycnocline around 200-300 m (Figure 7b) and have greater salinity (0.2 - 2.5 PSU) than normal and La Niña circumstances, notably in stations 1, 2, 3, 4, 5, and 6. In contrast to the other stations, stations 7 and 8 have warmer water masses and lower salinity. Temperatures range from 27 to 31 °C in station 7 and 18 to 31 °C in station 8. The temperature is 1–4 °C higher than during La Niña events and 2 °C higher than under normal circumstances. The deeper layer at each station follows a similar pattern to the upper layer.

The image below shows a typical stratification of IMC with its pycnocline property over the year and based on distinct monsoon periods during El Niño occurrences, similar to normal and La Niña situations. Table 4 summarises temperature and salinity conditions throughout El Niño occurrences.

During El Niño events, the top layer (100 m) and deeper layer (200 m) exhibit similar patterns. The Pacific Ocean experienced warmer conditions, ranging from 19 to 30 °C, than the IMC inlet (stations 2, 3, and 4 in Figure 1), while greater temperatures occurred at stations 5, 6, and 7. At the same time, station 8 (the Indian Ocean) exhibits a greater temperature range (18–31 °C) than the Pacific Ocean. During this event, the Pacific Ocean has a greater salinity of 34.0 - 35.4 PSU than the IMC (stations 2, 3, 4, 5, 6, 7) and the Indian Ocean, where the lowest (maximum) salinity is less than 34.0 (35.4) PSU. The deeper layer demonstrates that the Pacific Ocean and the Halmahera Sea had comparable salinity-temperature characteristics during this occurrence, which were 34.4 - 35.4 PSU and 11 - 23 °C, respectively. The comparison of the ITF paths from the Pacific Ocean to the Indian Ocean revealed a significant change in salinity and temperature in stations 5 and 7, particularly in the top to deeper layers. A warming process

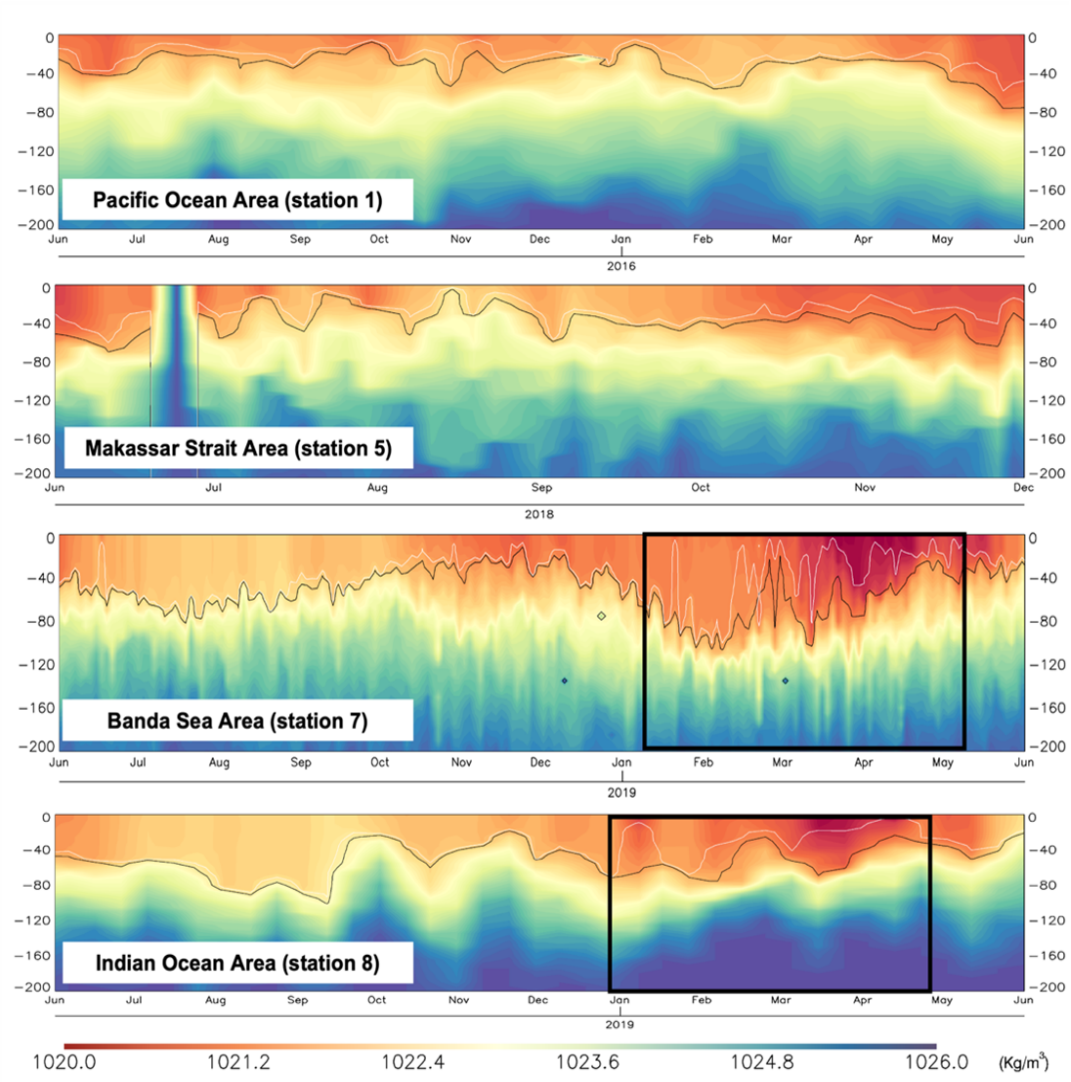

Figure 8. Density Profile in Several ITF Pathways during El Niño Events. This Time-Depth Illustration Shows Vertical Profile of Density Based on TS Diagram in the Figure 7. The Density Profile Is Overlaid with MLD in the White Line and ILD in the Black Line which Is Similar to Figures 4 and 6

may have happened in these stations since the top layer (deeper layer) temperature reached 25 – 30 °C (20 – 29 °C) at station 5 and 27 – 31 °C (20 – 27 °C) in station 7.

The Pacific Ocean, the northern water of North Molucca Island, and the Celebes Sea show that salinity values increase from SON (Figure 7c) to DJF (Figure 7d), although temperature characteristics reverse. The value difference between each stage of development is around 0.2 - 0.5 PSU and 1 - 2 °C. Stations 4 and 6 showed decreasing salinity and temperature from SON to DJF at 0.1 - 0.2 PSU and 1- 5 °C, respectively. During the peak phase of El Niño, the salinity and temperature parameters in the Makassar Strait and Java Sea became fresher due to warmer water mass. During SON, Makassar Strait and Java Sea were portrayed as having a salinity value of roughly 33.7 - 34.4 PSU, but this range altered to 33.6 - 34.0 PSU, and their temperature changed from 27 - 31 °C in SON to 30 - 31 °C in DJF. The increasing temperature of Makassar Strait is consistent with that of the Banda Sea, with an extreme change of roughly 7 °C (23 - 31 °C in SON to 30 - 31 °C in DJF), whereas salinity parameters in both SON and DJF are comparable, ranging between 34.1 and 34.4 PSU. The salinity and temperature of the Indian Ocean are generally lower than those of the Pacific. Salinity and temperature were lowered from SON to DJF by approximately 0.1 - 1 PSU and 1 oC, respectively. This ocean had a value of 34.2 - 35.0 PSU/16 - 30 °C (SON) to 33.2 - 34.9 PSU/15 - 30 °C (DJF). Because of the mixing and modification that occurs throughout the ITF channel, Pacific water masses that depart to the Indian Ocean are fresher than their original features.

Figure 8 depicts ocean dynamics at many sites by calculat-

ing MLD, ILD, and BLT, which are overlayed with density profiles, such as considerable upwelling in the Banda Sea from February to March and freshening waters during the northwest monsoon in the Banda Sea and Indian Ocean. In the Banda Sea, upwelling during El Niño peak periods is greater than during La Niña due to shallower ILD (20-30 m) compared to La Niña (40-50 m), as seen in Figures 6 and 8. Furthermore, BLT was seen during the northwest monsoon in this location, with a rise consistent with the existence of freshening anomalies in the waters (Napitu et al., 2015). It is also illustrated by the brown color gradation of low-density profile. Previous studies on the El Niño phenomena, notably in the Banda Sea, have shown that enormous upwelling causes a fall in SST approximately -0.5 to -1.5 °C followed by an increase in chlorophyll-a. La Niña induced a rise in SST in the Banda Sea, leading to weak upwelling (Iskandar, 2010; ?).

During El Niño, the Banda Sea, Indonesia's deepest basin, is thought to influence outlet pathways to the Indian Ocean, including the south of Bali Island and Southeast Nusa, due to massive upwelling (Setiawan et al., 2021). As seen in Figure 8, MLD in the Indian Ocean during the Northwest monsoon was shallower, about 5-30 m, and its freshening phases were comparable to the anomalies in the Banda Sea. According to Napitu et al. (2015), the depth of MLD paired with the atmospheric process determines the quantity of potential energy that depresses the ocean processes in modifying the heat content and contributes to controlling the strength of the surface flux on SST during El Niño.

4. CONCLUSIONS

During normal conditions, the northwest monsoon (DJF) period has a high salinity value in the inlet channel, whereas decreasing T-S in inlet regions occurs during the southeast monsoon (SON). Various variables, including upwelling and downwelling, as well as ENSO (La Niña and El Niño) occurrences, affect the mixing of ITF water mass during transit from station 1 to station 8. ENSO controls the depth components (MLD and ILD layer) through ocean-atmosphere interaction in MLD. El Niño causes a shallower depth component, while La Niña causes a deeper MLD layer. During La Niña in the Pacific Ocean, MLD appears at depths ranging from 80-120 m, whereas ILD shows up at shallower depths of up to 70 m. In the absence of ENSO and La Niña occurrences, notably in the northwest monsoon, Makassar Strait demonstrated an upwelling process in both situations. BLT was seen in all seasons, with a broader range during the northwest monsoon (February–March). Banda Sea, the deepest basin condition, has an ILD-MLD pattern of 10-50 m (without BLT), except for ENSO events during the northwest monsoon (BLT of 20-80 m). Furthermore, stronger upwelling was seen during El Niño occurrences compared to La Niña. The Indian Ocean has a shallow pattern of ILD-MLD along DJF, with a minimum depth of approximately 10 m in March and thick BLT along February during La Niña (MLD (ILD) is around 20-30 m (110-120 m)). BLT anomalies are also found throughout the El Niño event, with the MLD around 40-80 m and the ILD around 20-60 m.

5. ACKNOWLEDGMENT

The in-situ data is obtained from the Argo floats program and we thank to NOAA for providing the free data sources. This research is supported by the PMDSU Scholarship with contract number of 0195/UN9.3.1/PL/2023 from the Ministry of Research, Technology and Higher Education, Indonesia. We also thank you reviewers for the constructive comments resulting in a better paper.

REFERENCES

Agarwal, N., R. Sharma, A. Parekh, S. Basu, A. Sarkar, and V. K. Agarwal (2012). Argo Observations of Barrier Layer in the Tropical Indian Ocean. *Advances in Space Research*, **50**(5); 642–654

Aldrian, E. and R. Dwi Susanto (2003). Identification of Three Dominant Rainfall Regions within Indonesia and Their Relationship to Sea Surface Temperature. *International Journal of Climatology: A Journal of the Royal Meteorological Society*, **23**(12); 1435–1452

Atmadipoera, A., R. Molcard, G. Madec, S. Wijffels, J. Sprintall, A. Koch Larrouy, I. Jaya, and A. Supangat (2009). Characteristics and Variability of the Indonesian Throughflow Water at the Outflow Straits. *Deep Sea Research Part I: Oceanographic Research Papers*, **56**(11); 1942–1954

Bahiyah, A., A. Wirasatriya, J. Marwoto, and D. A. Anugrah (2019). Study of Seasonal Variation of Sea Surface Salinity in Java Sea and Its Surrounding Seas Using SMAP Satellite. In *IOP Conference Series: Earth and Environmental Science*, volume 246. IOP Publishing, page 012043

Banzon, V., T. M. Smith, T. M. Chin, C. Liu, and W. Hankins (2016). A Long-Term Record of Blended Satellite and in Situ Sea-Surface Temperature for Climate Monitoring, Modeling and Environmental Studies. *Earth System Science Data*, **8**(1); 165–176

de Boyer Montégut, C., J. Mignot, A. Lazar, and S. Cravatte (2007). Control of Salinity on the Mixed Layer Depth in the World Ocean: 1. General Description. *Journal of Geophysical Research: Oceans*, **112**(C6); 1–12

Drushka, K., J. Sprintall, S. T. Gille, and I. Brodjonegoro (2010). Vertical Structure of Kelvin Waves in the Indonesian Throughflow Exit Passages. *Journal of Physical Oceanography*, **40**(9); 1965–1987

Drushka, K., J. Sprintall, S. T. Gille, and S. Wijffels (2012). In Situ Observations of Madden-Julian Oscillation Mixed Layer Dynamics in the Indian and Western Pacific Oceans. *Journal of Climate*, **25**(7); 2306–2328

Feng, M., N. Zhang, Q. Liu, and S. Wijffels (2018). The Indonesian Throughflow, Its Variability and Centennial Change. *Geoscience Letters*, **5**(1); 1–10

Gordon, A. L. (1986). Interocean Exchange of Thermocline

Water. *Journal of Geophysical Research: Oceans*, **91**(C4); 5037–5046

Gordon, A. L. (2005). Oceanography of the Indonesian Seas and Their Throughflow. *Oceanography*, **18**(4); 14–27

Gordon, A. L. and R. A. Fine (1996). Pathways of Water between the Pacific and Indian Oceans in the Indonesian Seas. *Nature*, **379**(6561); 146–149

Gordon, A. L., J. Sprintall, H. M. Van Aken, D. Susanto, S. Wijffels, R. Molcard, A. Ffield, W. Pranowo, and S. Wirasantosa (2010). The Indonesian Throughflow during 2004-2006 As Observed by the INSTANT Program. *Dynamics of Atmospheres and Oceans*, **50**(2); 115–128

Gordon, A. L. and R. D. Susanto (2001). Banda Sea Surface-Layer Divergence. *Ocean Dynamics*, **52**; 2–10

Guo, Y., Y. Li, L. Cheng, G. Chen, Q. Liu, T. Tian, S. Hu, J. Wang, and F. Wang (2023). An Updated Estimate of the Indonesian Throughflow Geostrophic Transport: Interannual Variability and Salinity Effect. *Geophysical Research Letters*, **50**(13); 103748

Halkides, D., T. Lee, and S. Kida (2011). Mechanisms Controlling the Seasonal Mixed-Layer Temperature and Salinity of the Indonesian Seas. *Ocean Dynamics*, **61**(4); 481–495

Holte, J., L. D. Talley, J. Gilson, and D. Roemmich (2017). An Argo Mixed Layer Climatology and Database. *Geophysical Research Letters*, **44**(11); 5618–5626

Hosoda, S., T. Ohira, K. Sato, and T. Suga (2010). Improved Description of Global Mixed-Layer Depth Using Argo Profiling Floats. *Journal of Oceanography*, **66**; 773–787

Hu, S. and J. Sprintall (2016). Interannual Variability of the Indonesian Throughflow: The Salinity Effect. *Journal of Geophysical Research: Oceans*, **121**(4); 2596–2615

Hu, S., Y. Zhang, M. Feng, Y. Du, J. Sprintall, F. Wang, D. Hu, Q. Xie, and F. Chai (2019). Interannual to Decadal Variability of Upper-Ocean Salinity in the Southern Indian Ocean and the Role of the Indonesian Throughflow. *Journal of Climate*, **32**(19); 6403–6421

Iskandar, I. (2010). Seasonal and Interannual Patterns of Sea Surface Temperature in Banda Sea As Revealed by Self-Organizing Map. *Continental Shelf Research*, **30**(9); 1136–1148

Iskandar, I., D. Lestari, P. Utari, Q. Sari, D. Setiabudidaya, and W. Mardiansyah (2018). How Strong Was the 2015/2016 El Niño Event? In *Journal of Physics: Conference Series*, volume 1011. IOP Publishing, page 012030

Iskandar, I., D. O. Lestrai, and M. Nur (2019). Impact of El Niño and El Niño Modoki Events on Indonesian Rainfall. *Makara Journal of Science*, **23**(4); 7

Iskandar, I., P. A. Utari, D. O. Lestari, Q. W. Sari, D. Setiabudidaya, M. Khakim, I. Yustian, and Z. Dahlan (2017). Evolution of 2015/2016 El Niño and Its Impact on Indonesia. In *AIP Conference Proceedings*, volume 1857. AIP Publishing

Iskandar, M. R. and T. Suga (2022). Change in Salinity of Indonesian Upper Water in the Southeastern Indian Ocean during Argo Period. *Heliyon*, **8**(9); 1–12

Ismail, M., A. Taofiqurohman, and A. Purwandana (2020). Circulation Dynamics of the Banda Sea Estimated from Argo Profiles. In *IOP Conference Series: Earth and Environmental Science*, volume 584. IOP Publishing, page 012017

Jin, X. and J. S. Wright (2020). Contributions of Indonesian Throughflow to Eastern Indian Ocean Surface Variability during ENSO Events. *Atmospheric Science Letters*, **21**(8); 979

Kara, A. B., P. A. Rochford, and H. E. Hurlburt (2000). An Optimal Definition for Ocean Mixed Layer Depth. *Journal of Geophysical Research: Oceans*, **105**(C7); 16803–16821

Keerthi, M. G., M. Lengaigne, J. Vialard, C. de Boyer Montégut, and P. M. Muraleedharan (2013). Interannual Variability of the Tropical Indian Ocean Mixed Layer Depth. *Climate Dynamics*, **40**; 743–759

Koch Larrouy, A., G. Madec, D. Iudicone, A. Atmadipoera, and R. Molcard (2008). Physical Processes Contributing to the Water Mass Transformation of the Indonesian Throughflow. *Ocean Dynamics*, **58**; 275–288

Kusuma, D., A. Murdimanto, L. Aden, B. Sukresno, D. Jatisworo, and R. Hanintyo (2017). Sea Surface Temperature Dynamics in Indonesia. In *IOP Conference Series: Earth and Environmental Science*, volume 98. IOP Publishing, page 012038

Lee, T., S. Fournier, A. L. Gordon, and J. Sprintall (2019). Maritime Continent Water Cycle Regulates Low-Latitude Chokepoint of Global Ocean Circulation. *Nature Communications*, **10**(1); 2103

Lee, T., I. Fukumori, D. Menemenlis, Z. Xing, and L.-L. Fu (2002). Effects of the Indonesian Throughflow on the Pacific and Indian Oceans. *Journal of Physical Oceanography*, **32**(5); 1404–1429

Lee, T. and M. J. McPhaden (2008). Decadal Phase Change in Large-Scale Sea Level and Winds in the Indo-Pacific Region at the End of the 20th Century. *Geophysical Research Letters*, **35**(1); 1–7

Li, M., A. L. Gordon, L. K. Gruenburg, J. Wei, and S. Yang (2020). Interannual to Decadal Response of the Indonesian Throughflow Vertical Profile to Indo-Pacific Forcing. *Geophysical Research Letters*, **47**(11); 87679

Lu, X., S. Hu, C. Guan, M. Li, J. Sprintall, and F. Wang (2023). Quantifying the Contribution of Salinity Effect to the Seasonal Variability of the Makassar Strait Throughflow. *Geophysical Research Letters*, **50**(21); 105991

Makarim, S., J. Sprintall, Z. Liu, W. Yu, A. Santoso, X.-H. Yan, and R. D. Susanto (2019). Previously Unidentified Indonesian Throughflow Pathways and Freshening in the Indian Ocean during Recent Decades. *Scientific Reports*, **9**(1); 7364

Mardiansyah, W., D. Setiabudidaya, M. Y. N. Khakim, I. Yustian, Z. Dahlan, and I. Iskandar (2018). On the Influence of ENSO and IOD on Rainfall Variability Over the Musi Basin, South Sumatra. *Science and Technology Indonesia*, **3**(4); 157–163

McCreary, J. P., T. Miyama, R. Furue, T. Jensen, H.-W. Kang, B. Bang, and T. Qu (2007). Interactions between the Indonesian Throughflow and Circulations in the Indian and

Pacific Oceans. *Progress in Oceanography*, **75**(1); 70–114
Meehl, G. A. (1987). The Annual Cycle and Interannual Variability in the Tropical Pacific and Indian Ocean Regions. *Monthly Weather Review*, **115**(1); 27–50
Napitu, A. M., A. L. Gordon, and K. Pujiana (2015). Intraseasonal Sea Surface Temperature Variability across the Indonesian Seas. *Journal of Climate*, **28**(22); 8710–8727
Potemra, J. T. and N. Schneider (2007). Influence of Low-Frequency Indonesian Throughflow Transport on Temperatures in the Indian Ocean in a Coupled Model. *Journal of Climate*, **20**(7); 1339–1352
Santoso, A., M. H. England, J. B. Kajtar, and W. Cai (2022). Indonesian Throughflow Variability and Linkage to ENSO and IOD in an Ensemble of CMIP5 Models. *Journal of Climate*, **35**(10); 3161–3178
Setiawan, R., A. Wirasatriya, U. Hernawan, S. Leung, and I. Iskandar (2020). Spatio-Temporal Variability of Surface Chlorophyll-a in the Halmahera Sea and Its Relation to ENSO and the Indian Ocean Dipole. *International Journal of Remote Sensing*, **41**(1); 284–299
Setiawan, R. Y., Q. W. Sari, D. Setiabudidaya, N. Kurniawati, I. Iskandar, and E. Siswanto (2021). Surface Chlorophyll-A Variations along the Southern Coast of Java during Two Contrasting Indian Ocean Dipole Events: 2015 and 2016. *Journal of Sustainability Science and Management*, **16**(3); 116–127
Siswanto, F., D. Setiabudidaya, and I. Iskandar (2021). Surface Chlorophyll-a Variations along the Southern Coast of Java during Two Contrasting Indian Ocean Dipole Events: 2015 and 2016. *Journal of Sustainability Science and Management*, **16**(3); 116–127
Song, Q. and A. L. Gordon (2004). Significance of the Vertical Profile of the Indonesian Throughflow Transport to the Indian Ocean. *Geophysical Research Letters*, **31**(16); 1–4
Sprintall, J., A. L. Gordon, A. Koch Larrouy, T. Lee, J. T. Potemra, K. Pujiana, and S. E. Wijffels (2014). The Indonesian Seas and Their Role in the Coupled Ocean-Climate System. *Nature Geoscience*, **7**(7); 487–492
Sprintall, J., A. L. Gordon, S. E. Wijffels, M. Feng, S. Hu, A. Koch Larrouy, H. Phillips, D. Nugroho, A. Napitu, and K. Pujiana (2019). Detecting Change in the Indonesian Seas. *Frontiers in Marine Science*, **6**; 257
Sprintall, J. and A. Révelard (2014). The Indonesian Throughflow Response to Indo-Pacific Climate Variability. *Journal of Geophysical Research: Oceans*, **119**(2); 1161–1175
Sprintall, J. and M. Tomczak (1992). Evidence of the Barrier Layer in the Surface Layer of the Tropics. *Journal of Geophysical Research: Oceans*, **97**(C5); 7305–7316
Sprintall, J., S. E. Wijffels, R. Molcard, and I. Jaya (2009). Direct Estimates of the Indonesian Throughflow Entering the Indian Ocean: 2004-2006. *Journal of Geophysical Research: Oceans*, **114**(C7); 1–19
Suhadi, Supari, I. Iskandar, M. Irfan, and H. Akhsan (2023). Drought Assessment in Aceh and North Sumatra Using Effective Drought Index. *Science and Technology Indonesia*, **8**(2); 259–264
Supari, F. Tangang, E. Salimun, E. Aldrian, A. Sopaheluwakan, and L. Juneng (2018). ENSO Modulation of Seasonal Rainfall and Extremes in Indonesia. *Climate Dynamics*, **51**(7-8); 2559–2580
Syamsuddin, M. L., S.-I. Saitoh, T. Hirawake, S. Bachri, and A. B. Harto (2013). Effects of El Niño–Southern Oscillation events on catches of bigeye tuna (Thunnus obesus) in the eastern Indian Ocean off Java. *Fishery Bulletin*, **111**(2); 175–188
Tanaka, M. (1994). The Onset and Retreat Dates of the Austral Summer Monsoon Over Indonesia, Australia and New Guinea. *Journal of the Meteorological Society of Japan. Ser. II*, **72**(2); 255–267
Tozuka, T., T. Qu, Y. Masumoto, and T. Yamagata (2009). Impacts of the South China Sea Throughflow on Seasonal and Interannual Variations of the Indonesian Throughflow. *Dynamics of Atmospheres and Oceans*, **47**(1-3); 73–85
Tozuka, T., T. Qu, and T. Yamagata (2007). Dramatic Impact of the South China Sea on the Indonesian Throughflow. *Geophysical research letters*, **34**(12); 1–5
van Aken, H. M., I. S. Brodjonegoro, and I. Jaya (2009). The Deep-Water Motion through the Lifamatola Passage and Its Contribution to the Indonesian Throughflow. *Deep Sea Research Part I: Oceanographic Research Papers*, **56**(8); 1203–1216
Vranes, K., A. L. Gordon, and A. Ffield (2002). The Heat Transport of the Indonesian Throughflow and Implications for the Indian Ocean Heat Budget. *Deep Sea Research Part II: Topical Studies in Oceanography*, **49**(7-8); 1391–1410
Wang, S., C. C. Ummenhofer, D. W. Oppo, S. A. Murty, P. Wagner, C. W. Böning, and A. Biastoch (2023). Freshwater Contributions to Decadal Variability of the Indonesian Throughflow. *Geophysical Research Letters*, **50**(14); 103906
Wyrtki, K. (1961). Scientific Results of Marine Investigations of the South China Sea and the Gulf of Thailand 1959-1961. *NAGA Report*, **2**; 195
Wyrtki, K. (1987). Indonesian through Flow and the Associated Pressure Gradient. *Journal of Geophysical Research: Oceans*, **92**(C12); 12941–12946
Yulihastin, E. and N. T. Febrianti (2009). In Impacts of El Niño and IOD on the Indonesian Climate
Zhu, Y., L. Wang, Y. Wang, T. Xu, S. Li, G. Cao, Z. Wei, and T. Qu (2019). Stratified Circulation in the Banda Sea and Its Causal Mechanism. *Journal of Geophysical Research: Oceans*, **124**(10); 7030–7045

